# New Global Characterization of Landslide Exposure

Robert Emberson[1]

Dalia Kirschbaum[1]

Thomas Stanley[1,2]

5   Affiliations:

1. NASA Goddard Space Flight Center

2. Universities Space Research Association

**Abstract**

Landslides triggered by intense rainfall are hazards that impact people and infrastructure across
10   the world, but comprehensively quantifying exposure to these hazards remains challenging.
Unlike earthquakes or flooding which cover large areas, landslides occur only in highly
susceptible parts of a landscape affected by intense rainfall, which may not intersect human
settlement or infrastructure. Existing datasets of landslides around the world generally include
only those reported to have caused impacts, leading to significant biases toward areas with
15   higher reporting capacity, limiting how our understanding of exposure to landslides in
developing countries. In this study, we use an alternative approach to estimate exposure to
landslides in a homogenous fashion. We have combined a global landslide hazard proxy
derived from satellite data with open-source datasets on population, roads and infrastructure to
consistently estimate exposure to rapid landslide hazards around the globe. These exposure
20   models compare favourably with existing datasets of rainfall-triggered landslide fatalities, while
filling in major gaps in inventory-based estimates in parts of the world with lower reporting
capacity. Our findings provide a global estimate of exposure to landslides from 2001-2019 that
we suggest may be useful to disaster mitigation professionals.

## 1. Introduction

25   Rainfall-induced rapid landslides are an important natural hazard in many countries around the
world, both as independent events and within larger chains of cascading hazards due to their
role in downstream debris flow hazards. Current estimates of landslide impacts suggest that
they cause thousands of fatalities annually (Froude & Petley, 2018; Petley, 2012) and billions of
dollars of economic damage (Dilley et al., 2005). Global hazard estimates are an important way
30   to understand the relative efficacy of hazard mitigation mechanisms between different countries,
and also provide policy-makers with tools to estimate the future challenges associated with
landslide hazards. However, few studies exist at present that provide a globally-consistent set of
estimates for landslide hazard, and even fewer that attempt to characterize risk and exposure.

Most studies of landslide impacts rely on observations of specific landslide events and the
35     associated reporting of the impacts. A small number of studies have estimated global economic
impacts (Dilley et al., 2005; Guha-Sapir & CRED, 2019), while other important work has collated
the fatalities associated with landsliding around the world to give crucial insight into impacts
(Froude & Petley, 2018; D. Petley, 2012). The reliance of these studies on landslide inventories
leaves them subject to known biases associated with these inventories. Specifically, there tends
40     to be better reporting in developed countries (Kirschbaum et al. 2010; Monsieurs et al., 2018)
and a lack of public data about landslide occurrence and impacts in more remote regions,
resulting in major blind spots in Africa, portions of the Andes, western China, and parts of
Indonesia and the Philippines.

The global coverage of satellite data offers opportunities to fill in data gaps that result from
45     inventory-based assessment of landslide hazards. NASA's Landslide Hazard Assessment for
Situational Awareness (LHASA) model provides an estimate of landslide hazard between 50°N
and 50°S, at 30 arc-second resolution, based on a global susceptibility map and inputs from
NASA precipitation estimates (Kirschbaum & Stanley, 2018). This is updated every 3 hours, with
a latency of approximately 4 hours, providing a near-real time output. Using this model, it is
50     possible to estimate relative changes in landslide hazard around the world each year. More
importantly, this approach does not rely on local inventories to characterize the hazard, and
therefore provides a near-global, consistent estimate of landslide hazard, encompassing the
vast majority of populated areas. To address the need for globally consistent data on landslide
hazard and exposure, we utilize an updated and enhanced version of the global susceptibility
55     model defined by Stanley and Kirschbaum (2017) combined with a newly available 19 year
IMERG rainfall product (Huffman et al. 2014) to estimate global landslide hazard, and then
combine this with global estimates of population and critical infrastructure.

This information can also be considered together with other datasets such as Froude and Petley
(2018) to assess relative vulnerability to landslide exposure in different countries. A globally
60     consistent model could support hazard mitigation decision making and planning, particularly in
developing countries with limited reporting capacity. Our exposure model outputs derived from
the LHASA model provide an estimate of exposure seasonality at 30 arc second resolution
across the globe. This demonstrates the value of using remote sensing data in concert with
ground-based inventories to provide a more spatially consistent picture of the impacts
65     associated with landslides around the world. While the model outputs are an approximation of
exposure to hazard based on historical rainfall trends, we note that future exposure patterns
could be explored with the use of rainfall projections for future climate scenarios.

## 2. Methodology

70     To estimate exposure to landslide hazard, we must first derive the estimates of hazard itself. For
this study, we have utilised the outputs of an updated version of the LHASA model as an
approximation for hazard, which we can then combine with openly available datasets of
infrastructure at a 30 arc-second resolution across the world. These maps of exposure, both

annually and estimated for each month to analyse seasonal variability, are an important initial
75    output in their own right, but we have further analysed the data to compare our outputs with
existing estimates of global landslide hazard. This provides key insights into where existing
inventory biases may exist, as well as highlights which countries and regions are most exposed
to rainfall-triggered landslide hazard. Below, we detail the methods used to generate these
outputs.

80    **2.1. Hazard estimates derived from LHASA model**

The LHASA model is designed to provide near real time awareness of potential rapid landslide
activity through landslide 'Nowcasts' (Kirschbaum and Stanley 2018). The algorithm uses a
susceptibility map calculated from globally available estimates of slope, lithology, forest cover
change, distance to fault zones, and distance to road networks to provide a relative estimate of
85    static susceptibility (Stanley and Kirschbaum 2017). This susceptibility is divided into categories
based on decreasing area of the world occupied by each increasing class: this classification
scheme was designed so that each category was twice as large as the next highest, e.g., the
very low category contains roughly twice as many pixels as the low category. The susceptibility
map is then compared with satellite-based precipitation estimates from NASA's Tropical Rainfall
90    Measuring Mission (TRMM) Multi-satellite Precipitation Analysis (TMPA) and Global
Precipitation Measurement (GPM) Integrated Multi-satellitE Retrievals for GPM (IMERG) rainfall
product. To characterize the potential for landslide triggering, an Antecedent Rainfall Index
(ARI), or weighted accumulation from the last seven days of rainfall, is calculated at each pixel.
The weighting is an exponential weighting, with each day prior to the most recent multiplied by
95    $1/n^2$, where n is the number of days prior to present. The exponent value of 2 was calculated by
Kirschbaum and Stanley (2018) based on calibration at the locations of 949 landslides from the
years 2007-2013.

If the ARI value exceeds a threshold (historical 95th percentile for rainfall), either a moderate-
hazard or a high-hazard Nowcast may be generated if there is moderate to high susceptibility
100    within that area. Nowcasts are issued at a 30 arc-second (approximately 1km at the equator)
pixel resolution every 3 hours. For the purposes of our study, we use the daily nowcast output,
which is generated based on daily rainfall totals rather than 3-hr totals. The physical meaning of
one nowcast is 24 hours of elevated landslide hazard for a 30 arc-second dimension pixel.

We have updated the LHASA model for this study to incorporate data made available since the
105    initial version of the model. We term this revised model 'LHASA 1.1'. First, the global landslide
susceptibility map (Stanley & Kirschbaum 2017) was updated to include the 2018 data on forest
loss since the year 2000 (Hansen et al. 2018) and road density from the Global Roads Inventory
Project (Meijer et al. 2018). Previously, the forest loss data was modelled as a binary variable
representing either the presence or absence of any 30m forest loss pixel within each 30 arc-
110    second grid cell. However, this update represents forest loss at 30 arc-seconds  as a fraction of
the 30m grid cells which have recently experienced forest loss (from 2000-present). The effect
of this change will be to de-emphasize the role of forest loss in locations with little recent
disturbance, but not to change the effect of forest loss on any 30 arc-second grid cell which has
experienced total loss of all forest cover. The susceptibility map was recomputed at 30 arc-

115     second resolution using the same fuzzy overlay methodology as the previous version. This fuzzy overlay model uses heuristic weighting of the input variables, defined by Stanley & Kirschbaum (2017). We do not adjust the weights attached to the variables in the study here. We assess the accuracy of the new susceptibility map in the same fashion as in the study of Stanley & Kirschbaum (2017), by using the NASA Global Landslide Catalog locations to test the

120     ROC-AUC values. Using the same GLC data that was used to calibrate the previously published version of the susceptibility model (GLC data snapshotted 2016/01/14), we calculate an ROC-AUC value of 0.822, essentially identical to the value obtained for the prior model (0.82). For the purposes of our analysis, we follow Stanley and Kirschbaum (2017) and divide susceptibility into multiple classes, and use the threshold between 'low' and 'moderate' susceptibility as a

125     threshold for nowcasts to be generated if rainfall exceeds the historical 95th percentile. Less than 25% of landslides recorded in the GLC occur below this threshold. For the purposes of this study, we combine moderate and high 'nowcasts' together to provide a proxy for hazard that captures the bulk of landslide activity.

Secondly, we have updated the rainfall input.  Due to a recently released near 20-year record of

130     IMERG (version 6B), we have modified the precipitation inputs to LHASA in the following ways. First, we extend the LHASA model from 50 degrees N-S, which was the latitudinal extent of TMPA, to the 60 degrees N-S extent of the IMERG product (Huffman et al. 2013). This latitudinal expansion now includes most of Northern Europe and Canada, and the only populated areas excluded are in Northern Russia, Iceland, some of Scandinavia and Canada.

135     Because falling snow is an important component of precipitation at higher latitudes but not a major trigger of landslides, we changed the precipitation variable considered from total precipitation to just rainfall. The LHASA model does not consider snow avalanches. The effects of this change should be minimal in the tropical and temperate zones previously studied.

The LHASA model generates a hazard 'nowcast' if rainfall exceeds the historical 95th percentile

140     and susceptibility exceeds the 'moderate susceptibility' threshold. Since the updated model uses IMERG v06B rather than TMPA, we have therefore re-calculated the historical 95th percentiles of a 7-day weighted rainfall accumulation (based on 2000-present IMERG rainfall data). This provides a global 95th percentile map; if ARI values exceed this threshold, a hazard nowcast is issued. The model is then reprocessed from 2000-present, and we build a 19-year

145     record of landslide Nowcasts around the world. Averaging the Nowcasts by month, we construct a Nowcast climatology, or average landslide Nowcast rate for each pixel. We also compute annual Nowcast rates. This provides a globally consistent proxy for landslide hazard over the course of the year in each location. We term this as 'Nowcast density', and it represents a proxy for intensity of landslide activity. We can then combine this with data on population and

150     infrastructure to assess the relative exposure to landslides.

The result is a raster dataset at 30 arc-seconds resolution for each month of the years in the IMERG record. We compute additional metrics such as the inter-annual variability in Nowcast frequency and standard deviations of Nowcast frequency. This information is incorporated into the annual exposure estimates to provide a measure of the variability. This uncertainty analysis

155     is discussed in more detail below.

## 2.2. Exposure datasets & integration with hazard

We have overlaid the hazard footprints derived from the LHASA-based Nowcast climatology on top of publicly available datasets of population and infrastructure globally to map the exposure of these elements to landslide hazard. We have additionally aggregated these data at a national scale to compare with existing studies. Below, we first describe the datasets used, and then the approach taken to combine them with the hazard outputs.

We use population data from the Gridded Population of the World version 4 dataset (Doxsey-Whitfield et al., 2015), adjusted to the UN WPP Population Density for 2015. Use of this dataset is in line with other studies of population exposure to global hazards (Carrao, Naumann, & Barbosa, 2016; Dilley et al., 2005; Kleinen & Petschel-Held, 2007). The resolution of this dataset is the same as the LHASA Nowcast output – 30 arc-seconds – and thus can be directly mapped onto the hazard data.

The definition of critical infrastructure can differ depending on the relevant stakeholder or location. The UN Global Assessment Report 2015 incorporates schools, hospitals and residential areas (De Bono & Chatenoux, 2014), and we use this as an initial basis for our estimates. We incorporate roads as defined in the Global Roads Inventory Project (GRIP) (Meijer et al., 2018), and amenities including hospitals, schools, fuel stations and power facilities as defined by OpenStreetMap. Both catalogs have a global extent and are updated regularly. Additionally, they offer a consistent set of data that can be compared across the world. While there are some caveats to this comparison, which are discussed below, we suggest that these two datasets are likely the best datasets with global coverage, open access, and recent updates.

The GRIP roads dataset harmonises nearly 60 datasets describing road infrastructure into a single, consistent dataset covering 222 countries (Meijer et al. 2018). GRIP incorporates roads derived from OSM as well as other data sources, and is considered to be a harmonised global road catalog. The daily updates for OSM are not incorporated into GRIP, but we consider the globally harmonised nature to be more important than a frequently updated catalog for the purposes of our study. This dataset is a shapefile of linear features, which is not initially directly compatible with the 30 arc-second resolution landslide hazard outputs.  To connect the linear road dataset with the pixel-based Nowcast based landslide hazard data, we have used the Line Density tool in ArcGIS to calculate the density of roads at 30 arc-second resolution with an output of a road density map with units of $km/pixel^2$. Although the GRIP database classifies roads in one of five classes depending on size and importance (e.g. primary highway, residential road), we have not distinguished between these classes in our analysis. This dataset does not include footpaths or unpaved roads, for which mapping may be significantly more spatially inconsistent. While economic impacts vary based on the type of road, our analysis is meant to highlight the total potential exposed length for all types of roads.

OpenStreetMap (OSM) is a continually updated global map of infrastructure, roads, settlement and land uses (OpenStreetMap contributors 2015). The updates are contributed by members of the public and the data is openly available for access in shapefile and XML format. While

differing levels of input from different parts of the world mean that there can be differences in the level of completeness of the map depending on the region (Barrington-Leigh and Millard-Ball 2017), the specificity of the data makes it an excellent source for infrastructure information. There is detailed classification of different features in the map that allow us to isolate specific

200    types of infrastructure, such as medical amenities or power stations. In addition, the open-source nature of OSM means this approach is highly replicable. We have used the OSM Planet data file (a single XML document of approximately 1TB, containing the information for every mapped feature in the OSM map) and parsed the xml data using a Python-based script to obtain the density of critical amenities at a 30 arc-second resolution. We define critical amenities

205    as those labelled 'School', 'Hospital' 'Fuel Station', 'Power Station' and other 'Power' nodes (including substations and transformers), based on the OSM feature definitions. We count each node as a single point, providing a density estimate of 'nodes [school or hospital, etc] per 30x30 arc second cell', where nodes are of the types defined. The OSM Planet file was downloaded on June 24th 2019. The script used to parse this file is available in the supplementary material.

210    To combine the roads datasets and OSM-derived critical infrastructure with the hazard outputs, we have multiplied the raster map of infrastructure or road density by the Nowcast density raster (i.e. raster showing total days exposed to landslide hazard) for each full year in the IMERG archive (2000-2018) and taken the mean value and standard deviation. The resulting datasets on exposure for population, roads, and critical infrastructure are all calculated at 30 arc-second

215    resolution. We have also generated month-by-month exposure rasters to estimate the climatology of exposure for the same exposed elements. Since these outputs are based upon the LHASA Nowcast output, it is important to clarify the units in which our estimates of exposure are expressed. Table 1 provides a summary of the units and the terms used in the study.

| Parameter | Specific Unit | Descriptive term (shorthand used in this study) | Explanation |
|---|---|---|---|
| Population exposure | Days exposed to landslide hazard. person . $Yr^{-1}$ / 30x30 arc-second cell | $Pop_{exp}$ | The exposure is estimated as number of Nowcasts (i.e. days exposed to elevated modeled hazard) per year in each square km multiplied by the population in that 30x30 arc-second cell. |
| Road exposure | Days exposed to landslide hazard .km.$yr^{-1}$/ 30x30 arc- | $Road_{exp}$ | Sum of Nowcasts per square km multiplied by km of road in |

| | second cell | | that 30x30 arc-second cell. |
|---|---|---|---|
| Infrastructure exposure | Days exposed to landslide hazard.element.yr$^{-1}$/ 30x30 arc-second cell | Infr$_{exp}$ | Includes the following critical infrastructure categories: hospitals, schools, fuel stations, power generation and transmission |

*Table 1: Summary of terms used to describe infrastructure and associated units.*

220    In Table 1, the units for each of the exposure outputs is also explained. We use the shorthand Pop$_{exp}$, Road$_{exp}$, and Infr$_{exp}$ to denote population, road and infrastructure exposure respectively.

**2.3. Error assessment**

Kirschbaum and Stanley (2018) assess errors in the LHASA 1.0 Nowcast hazard estimates by comparison with historical landslide events recorded in both the NASA Global Landslide Catalog
225    (Kirschbaum et al., 2010) and the dataset of fatal landslides generated by Petley et al. (2007). They find relatively low False Positive Rates (~1%) and moderate to good true positive rates (24-60% for moderate hazard Nowcasts). However, both the Global Landslide Catalog and the data of Petley et al. (2007) are not complete, meaning that the true and false negative rates are not easily quantified. More succinctly, since a complete dataset of landslide occurrence does
230    not exist, it is challenging to calculate the accuracy associated with any independent landslide hazard estimate. Quantifying the relationship between Nowcast density and landslide probability for a given area remains an important step for future research, and requires spatially complete landslide catalogs with high temporal revisit rates. To explore the relative variability in landslide activity, we estimate the standard deviation in annual Nowcast density at each point, based on
235    the 19 year IMERG rainfall input. We then propagate the error into the estimates of exposure for population, roads and critical infrastructure. The raster data for the standard deviations in error are available in the supplemental data.

Estimating errors associated with OpenStreetMap data can be challenging, since the data quality is determined by volunteers who contribute to the map database. Broadly, we suggest it
240    is appropriate to consider two distinct sources of error; the location accuracy of the individual points and infrastructure, and the completeness of the inventory. As discussed by Mooney and coauthors (2010), a lack of ground data across the world makes it challenging to assess the positional accuracy. However, in some locations, data can be compared with existing sources. In the UK, Haklay (2010) suggests that OSM data points offer positional accuracy comparable
245    with the Ordinance Survey Maps (the government standard). For the purposes of our study, where the maximum resolution available for the landslide hazard data is 30 arc-second, this positional accuracy is in excess of the requirements. However, completeness of the map is more problematic.

Barrington-Leigh and Millard-Ball (2017) assess the relative completeness of the OSM roads
data on a country-by-country basis, finding that OSM data in many developed countries is near-
complete, although this declines in some states with lower GDP. The completeness varies
within individual countries, with the most complete mapping observed in the highest density
cities as well as the most sparsely populated areas (reaching a low in moderately populated
areas). We assume that the estimate of completeness presented by Barrington-Leigh and
Millard Ball (2017) for roads is applicable to other infrastructure; we are not aware of other
global estimates of OSM completeness for specific infrastructure categories, so while this
assumption may not fully hold we suggest it is more informative to use this completeness
estimate than none at all. Note that this also assumes completeness is consistent within
individual countries. The OSM completeness estimates are calculated at a national level, and it
is therefore not clear how to apply them to the 30 arc-second pixels in our study, and as such
we do not attempt to correct our global maps. However, to effectively normalise the exposure
data at a country level, we provide the completeness measure derived from Barrington-Leigh
and Millard-Ball (2017) in Supplementary Table 1. In the figures in supplementary material that
show $Infr_{exp}$ aggregated at a national level, we normalise the exposed elements by the total
number of critical infrastructure elements in each country, which serves to provide a useful
intercomparison of the relative hazard, and does not require completeness metrics.

The GRIP roads database (Meijer et al. 2018) draws a significant part of the road inventory from
OpenStreetMap, and so is subject to some of the same error constraints. In Europe, the roads
are derived primarily from OSM, although completeness in this part of the world is near-perfect
(Barrington-Leigh and Millard-Ball 2017). GRIP also uses OSM data in China, where there is a
dearth of other freely available datasets. As such, completeness estimates in China are difficult
to accurately characterize, and we do not attempt to do so. Elsewhere, GRIP incorporates other
road datasets to supplement OSM. These input datasets are limited to those with positional
accuracy greater than 500m, which precludes significant positional errors that would affect our
km-scale analysis. We are not aware of estimates of the completeness of the GRIP dataset;
since it integrates datasets from all over the world, external validation datasets of completeness
are unlikely to exist comprehensively. As such, while we note that there may be parts of the
world where coverage is incomplete, we do not have strong constraints on this.

## 3. Results

The results of our analyses provide a global set of model estimates of landslide exposure, in
both raster format and tabulated by country. The source data is available in the supplementary
material associated with this study.

Figure 1 shows the modeled estimates of population exposure annually for each 30 arc-second
pixel and Figure 2 shows the exposure of population, roads, and critical infrastructure at the
same scale for a portion of Northern Italy and the Alps, to highlight the nature of the different
datasets. As can be observed in Figure 2, population and roads are significantly more widely
distributed than critical infrastructure. Infrastructure is instead concentrated primarily in urban

290 centers, although power distribution infrastructure follows similar transportation corridors to road networks. In other parts of the world, there are significant levels of exposure of critical infrastructure to landslide hazard. The co-location of power distribution and road network exposure highlights the potential for complex post-landslide damage and multi-sector impacts.

295
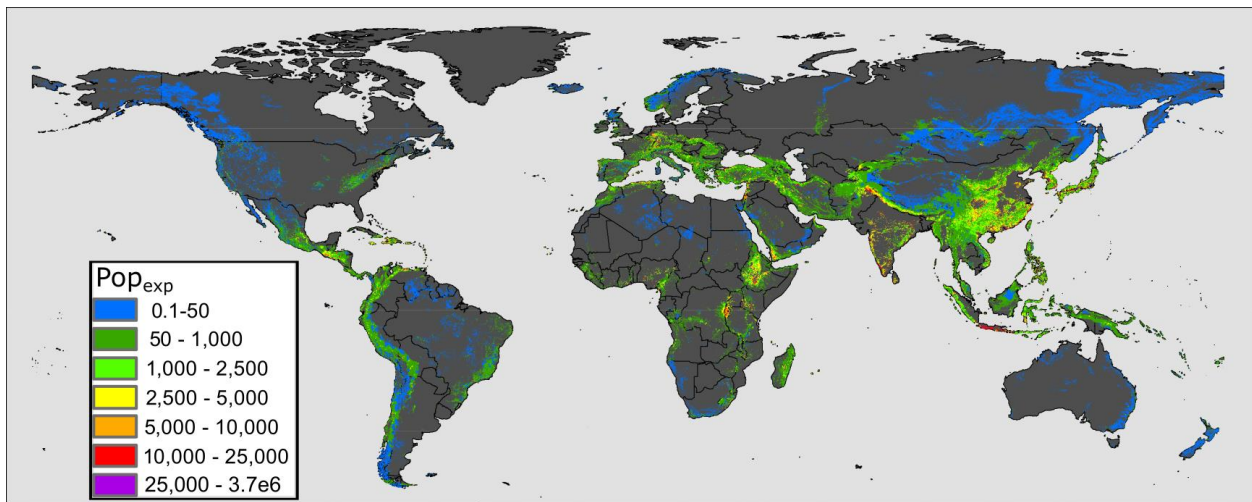
*Figure 1: Global modeled population exposure to landslides ($Pop_{exp}$). Since the distribution of high-exposure areas is highly localised, we have binned the data to highlight differences at lower exposure levels more clearly.*

300
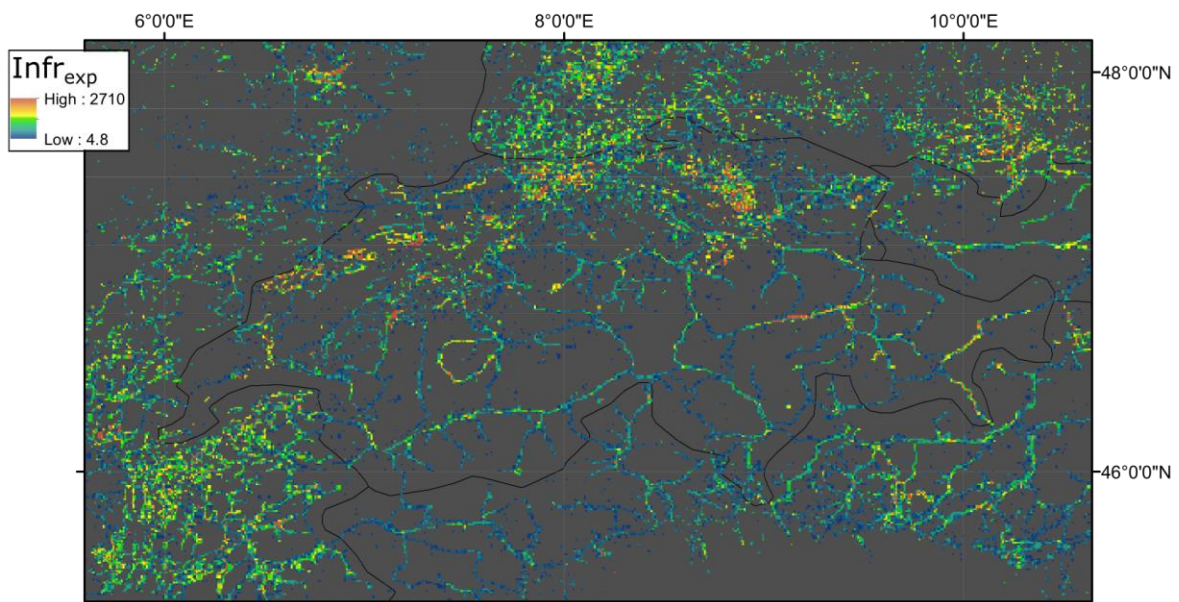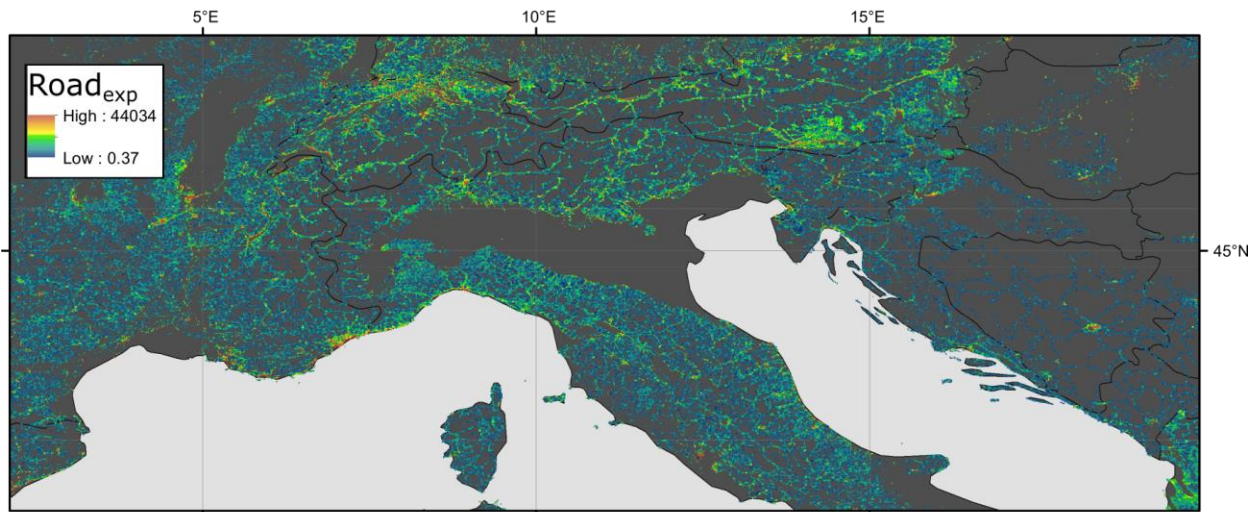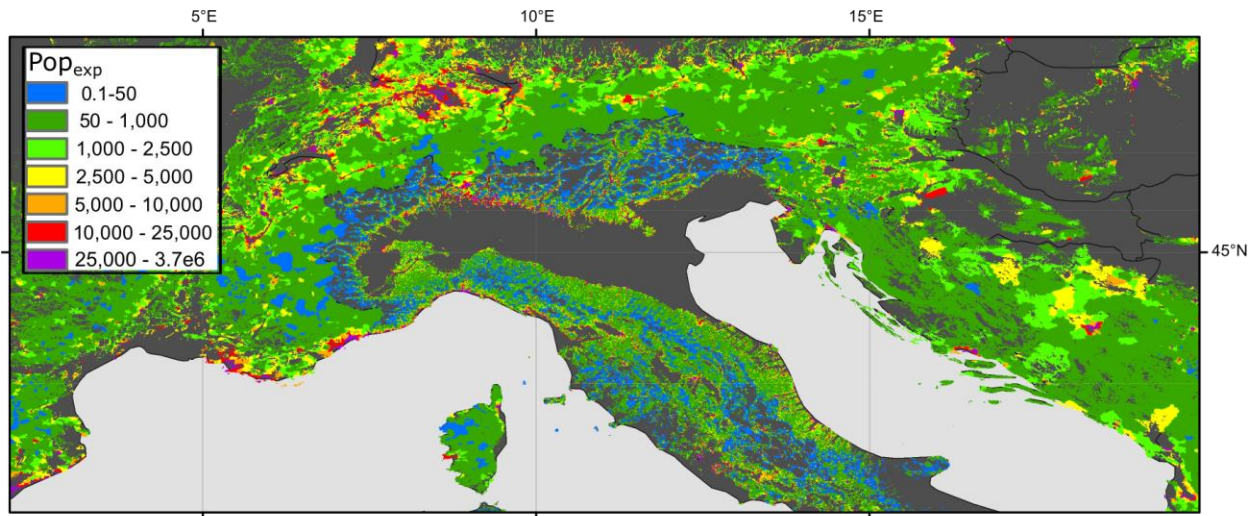
*Figure 2: Showing relative exposure of population, critical infrastructure, and roads in a*

305    *snapshot of the world map - in this case, the European Alps and Italy. To improve clarity, the*
      *critical infrastructure exposure is shown only for Switzerland.*

      For each country we have tabulated the aggregated values for $Pop_{exp}$, $Road_{exp}$, and $Infr_{exp}$,
      average annual Nowcast density. We also show the total population, total length of roads from
310   GRIP, and total number of OSM critical infrastructure elements; this allows for calculation of the
      fraction of total that are exposed for each of these aspects. To normalize the number of
      Nowcasts for each country, we divide by area in square decimal degrees, rather than square
      kilometers; since the Nowcast data is output on a grid based on decimal degrees. The same
      aggregation approach could similarly be used at a sub-national level to assess relative impacts
315   in different administrative areas. These data can be found in Supplementary Table 1, where all
      data necessary to replicate these results is available.
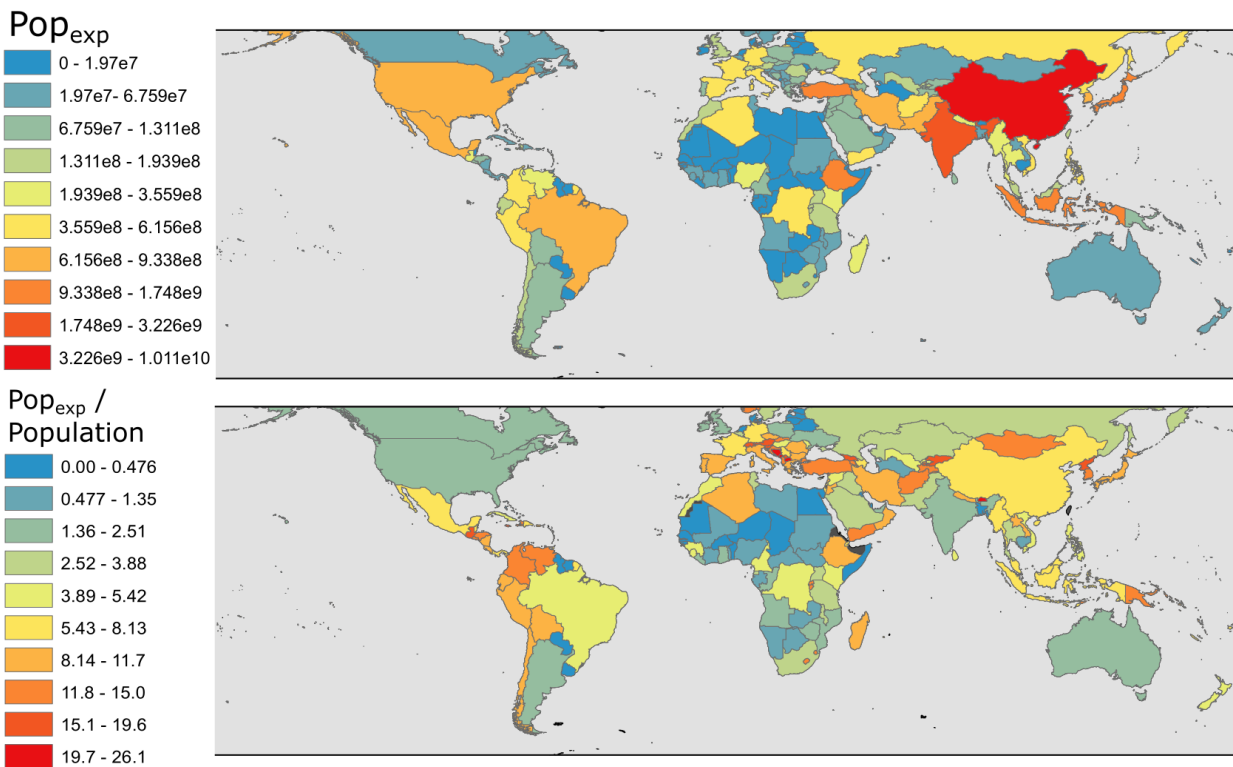
*Figure 3: Above: Country wide estimates of Population exposure ($Pop_{exp}$); Below: Population*
*exposure normalised by total population. This is expressed as $Pop_{exp}$ divided by total 2018*
320   *population derived from the World Bank data archives (World Bank 2018). Countries in black in*
      *lower figure lack World Bank population estimates.*

      Figure 3 plots the absolute numbers for $Pop_{exp}$, as well as the relative fraction of the population
      impacted by landslides. The relatively lower values in some of the larger countries like the
      United States and Brazil suggests that while the overall population impact is high in highly
325   populated states, the relative impact can be more concentrated in smaller countries.

We also list the OSM completeness estimates from Barrington-Leigh and Millard-Ball (2017), the fatalities per country due to non-seismic landslides assessed by Froude and Petley (2018), and the landslide-linked economic impacts assessed by Dilley et al (2005). These datasets are,

330 to our knowledge, the most current datasets that assess landslide impact in terms of economic cost and fatalities globally, and provide valuable points of comparison for our results.

## 4. Discussion

The most striking initial result of our study is that significantly larger proportions of the globe are exposed to rainfall-triggered landslide hazards than are often considered (Figure 1). Inventory

335 based assessments (e.g. Dilley et al. 2005) do not show significant levels of landslide hazard and exposure in sub-Saharan Africa or much of Asia and South America, while we find that many of these countries have significant proportions of the population and infrastructure exposed. It is perhaps not surprising that exposure to landslide hazard is elevated in the major mountain belts of the Andes and the Alpine-Himalayan Orogeny, but there are other key

340 hotspots that may be less well known. These areas include much of Japan, the Rwenzori mountains in Africa, Central America and Mexico, and much of the Caribbean. We find specific hotspots for certain cities within or near mountain belts; this is particularly evident at the edges of large conurbations that abut mountainous areas, such as Taipei, Rio de Janeiro and the edges of Tokyo.

345 While the zones of densely packed critical infrastructure such as schools and hospitals are also in general associated with these urban areas, the exposure of linear infrastructure to landslides is more widespread. Roads and power transmission facilities often follow similar linear corridors, and where those intersect areas of high landslide hazard the relative exposure can still be important. The localised impact of a single landslide impacting a densely populated urban zone

350 may be very high, with several critical infrastructural elements impacted. However, the likelihood of a landslide occurring somewhere along lengthy road or power transmission segments in regional-scale rainfall events is higher, and an interruption to linear infrastructure may impact lifelines that are relevant in disaster response. Thus the localised and distributed impacts should be considered alongside one another, We suggest that highlighting the most vulnerable

355 corridors for power transmission and road traffic is an important subject for future work.

To explore these results against independent datasets of landslide hazard and risk, we have aggregated the data at a country level (Supplementary Table 1). We can then highlight those nations with the highest landslide impact both in absolute terms (total exposed people and infrastructure) and as a proportion of the overall population or infrastructure in that country.

360 As might be expected, without normalising for area countries with the largest population have the highest overall modeled population exposure, although exposure in China exceeds that of India despite having a smaller population. Exposure of roads is also greatest in China and the United States, which are both highly populated with good OSM coverage. These absolute values are important, but we suggest that more insight can be gained by assessing the relative

365    exposure of population and infrastructure in each country, as well as by comparing the different relative values between nations.

Inter-comparison of different countries can highlight those nations where the impact of landslides is greatest, and can draw attention to smaller, less developed nations where landslide statistics from report-based inventories may be lacking.

370
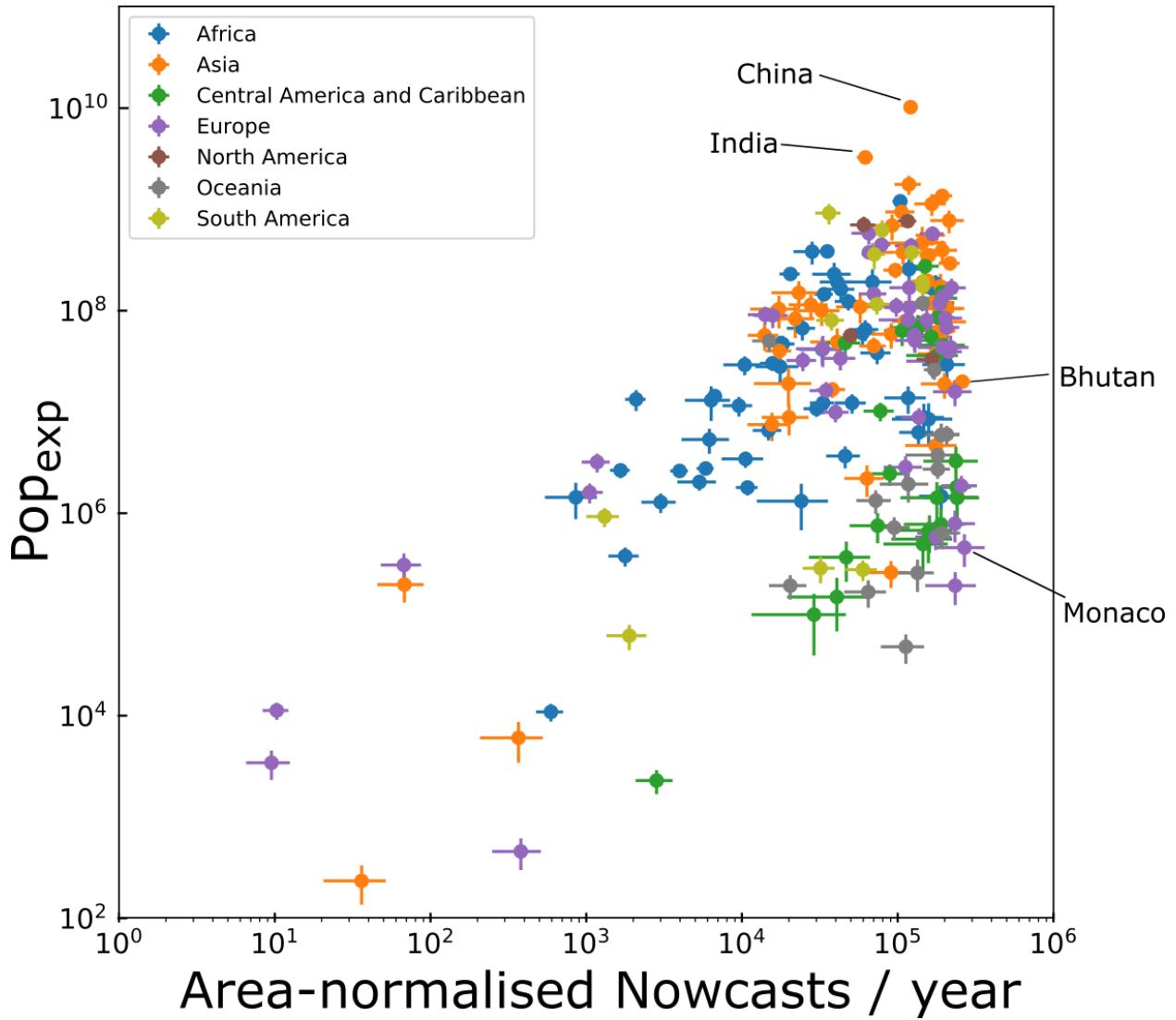
*Figure 4: Nowcasts per year, normalised by country area compared with the population exposed to Nowcasts (in units of Nowcast/person-years).*

Figure 4 plots $Pop_{exp}$, against the mean nowcast density in that country, with colors denoting the
375    geographic region. Results indicate that hazard and exposure are generally well-correlated across different countries; similar relationships exist for both road exposure and critical infrastructure (see supplementary material for figures). At the highest end of this scale – i.e.

those with high x-axis values - are smaller countries where mountainous terrain makes up much if not all of the area: Monaco, Bhutan, Andorra, and several Caribbean States: St Vincent and the Grenadines, Dominica, Grenada and St Lucia. In terms of population exposure, many countries in Asia and Africa have higher population exposure for an equivalent level of Nowcast density, when compared to European and some central American countries. This results from the generally higher population of these states.

Given the large degree of variability in annual Nowcast frequency, inventories of reported landslides may misrepresent the average landslide rate in smaller countries if catastrophic landslides do not coincide with the sampling period for the inventory. At the same time, the LHASA-based model outputs are relatively insensitive to extreme rainfall events (100-year return period, for example), since all rainfall values above the 95th historical percentile will lead to the same nowcast hazard output. The bulk of reported landslide events occur in larger nations where statistical variability of landsliding is likely damped over larger areas like Nepal, Taiwan, China and Japan. While we find high normalised hazard estimates in many of those states, our analysis also highlights smaller nations where the relative impact of landslides may be more significant on longer timescales. Alongside the previously mentioned nations, we also find several smaller states with higher proportions of exposed population; Montenegro, Bosnia and Herzegovina, and Macedonia are notable in the Balkan area in particular.

To test whether the Nowcast-exposure estimates are a useful predictor of landslide risk, we can compare them to existing datasets. In Figure 5, we plot the total exposure of population in each country (in units of person-Nowcasts per year) against the landslide fatality dataset assembled by Froude and Petley (2018). This dataset, collected from 2004-2016, consists of 4862 separate landslide events that resulted in fatalities, and is the most comprehensive dataset for landslides that have caused fatalities in the world. Figure 5 highlights that there is a relatively strong correlation, with countries in Asia, Central America and Africa generally exhibiting higher numbers of fatalities for a given population exposure than observations in Europe.
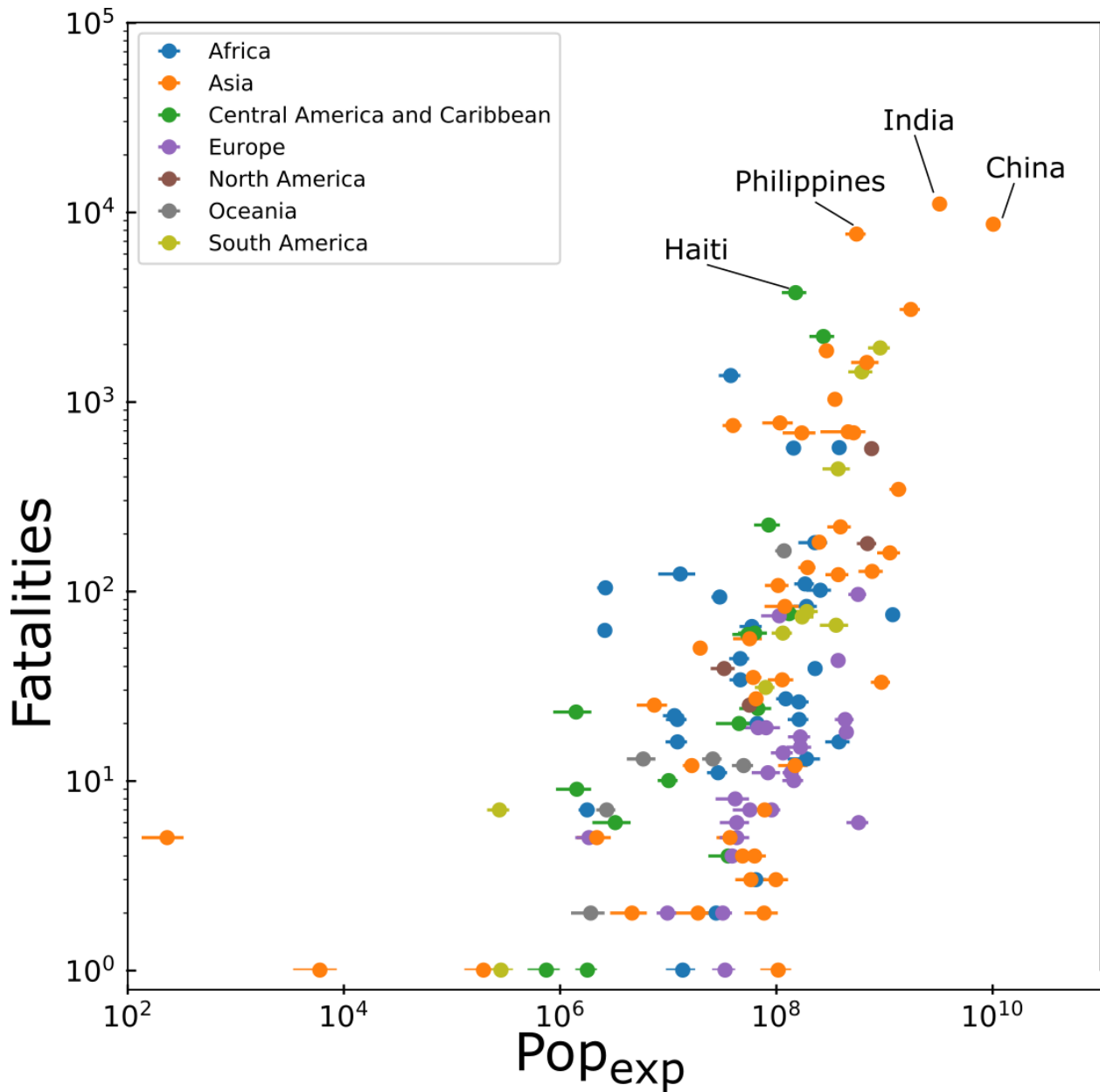
*Figure 5: Showing the exposure of population (in person-Nowcasts/year) against the number of total fatalities recorded in the dataset of Froude and Petley 2018*

In Figure 6, we plot the total road exposure against a derived metric of GDP impact from Dilley et al. (2005) based on the EM-DAT landslide dataset. The EM-DAT based assessment divides the globe into 2.5 degree squares and does not present absolute values of total economic loss, but instead a relative decile (1-10 with increasing risk) ranking of grid cells based upon the calculated economic loss risks. While this metric is not quantitative of the economic risk, we suggest that it is possible to compare these relative loss rates against our results. As with the comparison between $Pop_{exp}$ and fatalities, we see a relatively strong correlation. However, it is clear that the EM-DAT dataset is incomplete; the complete absence of data on costs associated

with landslides in African countries limits how effectively we can compare this inventory with our model estimates. The absence of data further highlights the value of our globally consistent approach.

420
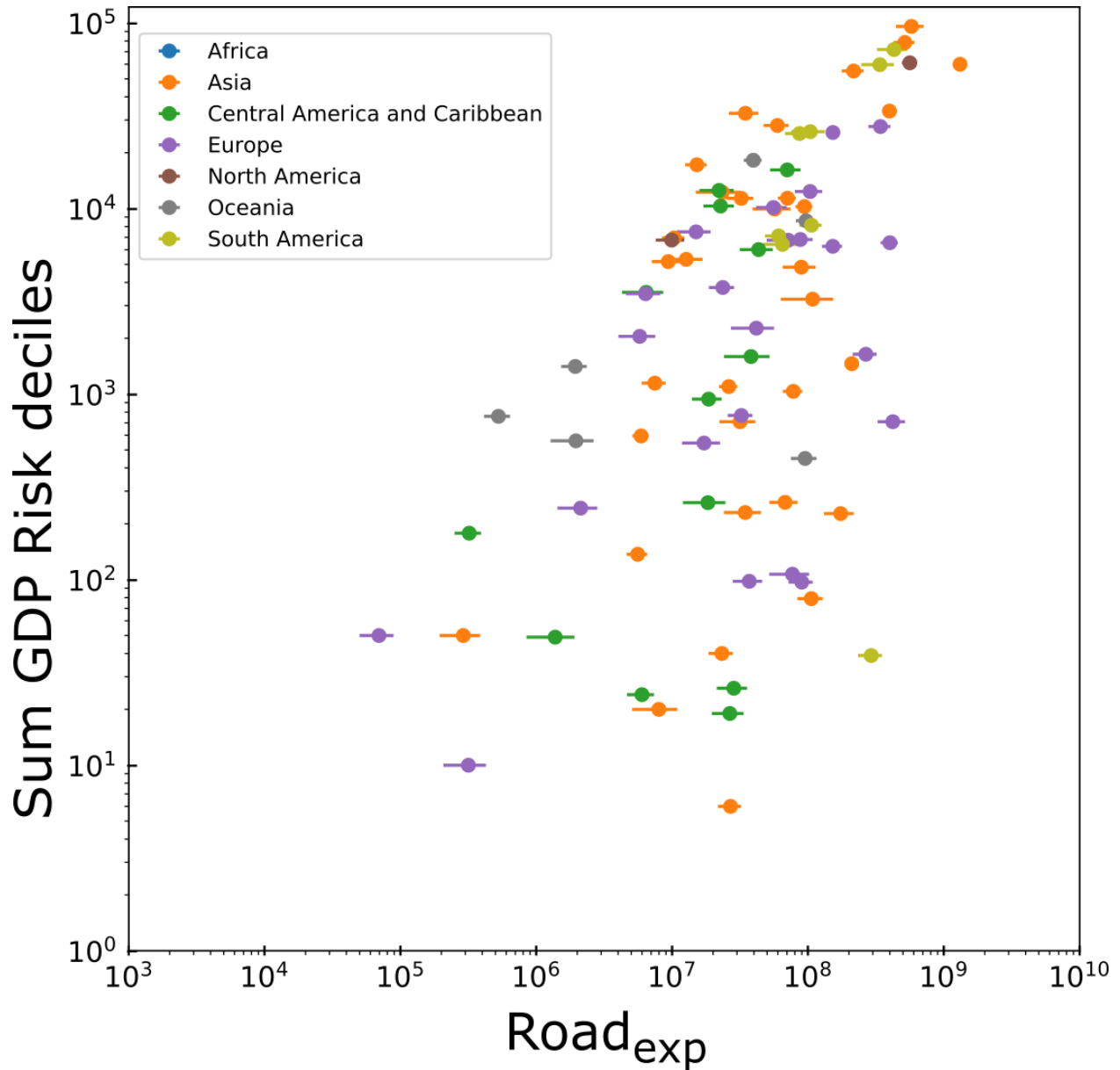
*Figure 6: Plotting the exposure of roads (in road-km Nowcasts / year) against the estimated GDP cost of landslide impact estimated by Dilley et al. (2005).*

425    Although there are countries without data in the EM-DAT derived database, it may be possible to derive these missing values based on the relationship between $Road_{exp}$ and the countries

where EM-DAT data exists (points in Figure 6) – i.e., to capture the y-axis values based on a known x-axis value. However, the degree of scatter evident in Figure 6 suggests that further data is required to explicitly define such a relationship, and error margins may be large.

430 Extrapolation and validation of this relationship is beyond the scope of this current work, but we suggest is an important topic for future research.

In order to learn which factors control the relationships between exposure and impact in different countries, we can combine the inventory data with our estimates and compare it with other variables. In Figure 7, we plot the number of fatalities recorded in the dataset of Froude

435 and Petley (2018) divided by $Pop_{exp}$. This is subdivided by continent. We suggest that fatalities divided by exposure provides a proxy for the degree of hazard mitigation in a given country; lower values indicate that for a given level of population exposure, fewer fatalities are observed. We find high variability in each continent, although in general there are lower levels of fatalities per unit exposure in Europe when compared to Central America and the Caribbean, as well as

440 South America. Germany and Hong Kong, highly developed countries, have proportionally low fatalities despite high levels of exposure, which we speculate is likely a result of extensive mitigation efforts.
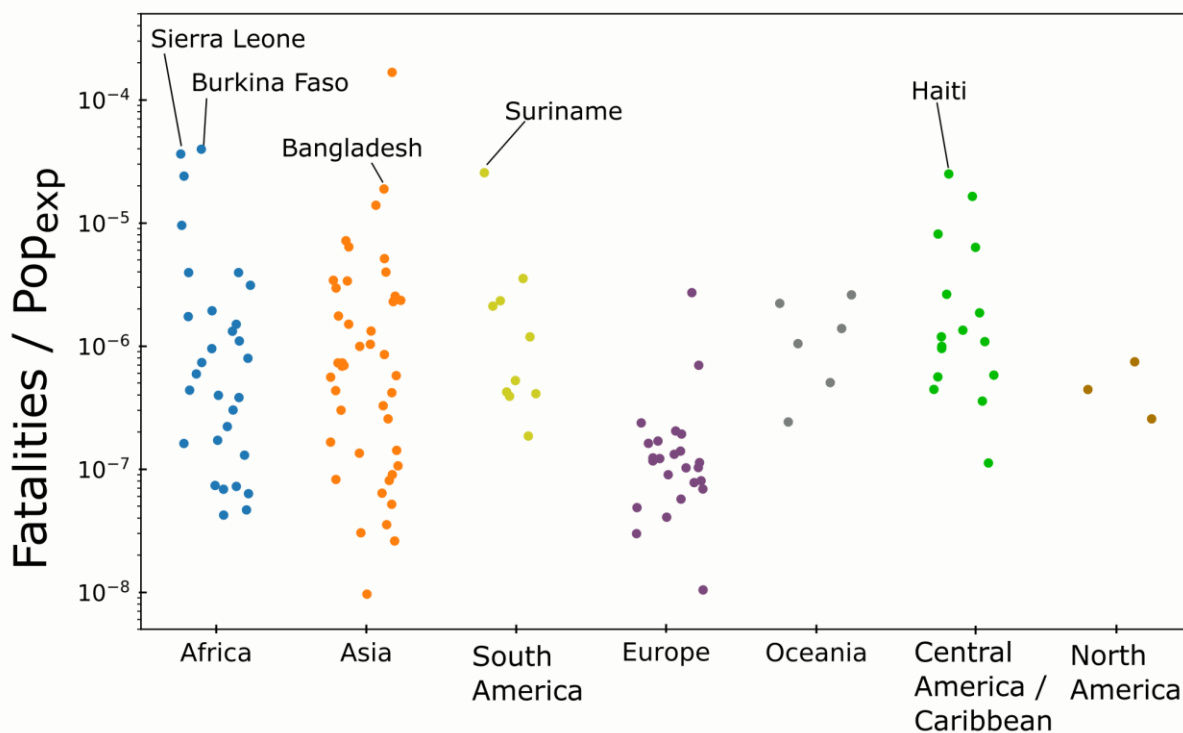
445

*Figure 7: Number of fatalities divided by Pop$_{exp}$, for each continent. The wide spread of values in Africa and Asia are likely a reflection of the diversity of nation-to-nation landslide vulnerability. Offsets in the x-axis are for visual distinction between points to avoid overlap.*

450 At the other end of the spectrum, some less developed countries exhibit higher fatalities for a given exposure; Sierra Leone, Burkina Faso, Haiti, Suriname, Bangladesh, Dominica and the Philippines have a significantly higher level of fatalities per unit of exposure. Some key outliers (Qatar and Bahrain) have high fatality per unit exposure, but these nations have very low overall exposure (see Supplementary Table 1) meaning that even a small number of fatalities increases the y-axis value in Figure 7 to a large degree. This analysis, while not at this stage
455 comprehensive, potentially allows us to explore a proxy for national-level risk management associated with landslide hazard, or relative vulnerability to a given level of exposure

To explore whether the variability in fatalities divided by Pop$_{exp}$ seen in Figure 7 is related to the level of development in each country, we have compared fatalities / Popexp with 2018 GDP values for each country (World Bank 2019) *A priori*, we would expect countries with greater
460 GDP to be capable of mitigating hazard more effectively, and thus have fewer fatalities for a given level of exposure. However, while there is a small average decline in fatalities for a given exposure as GDP increases (Figure 8), with some high GDP countries showing the lowest fatality values (notably Germany and Hong Kong) there is a significant degree of variability in this relationship, suggesting there is a more complex relationship.

465 We note that comparing the model-based estimates of exposure with the fatality inventory of Froude and Petley (2018) in this manner may lead to erroneous conclusions if not considered carefully. While it is likely that many, if not all of the fatal landslides in developed countries are accurately recorded, this may not be the case in states where disaster management is less advanced. As such the lack of strong relationship between fatalities per unit exposure and GDP
470 per capita observed in Figure 8 may represent gaps in the data in countries with lower GDP per capita, and thus a systematic bias within this analysis. Phrased differently, there may still be a relationship between GDP and fatalities for a given exposure level, but this may be masked by a lower reporting capacity in less-developed nations.

475
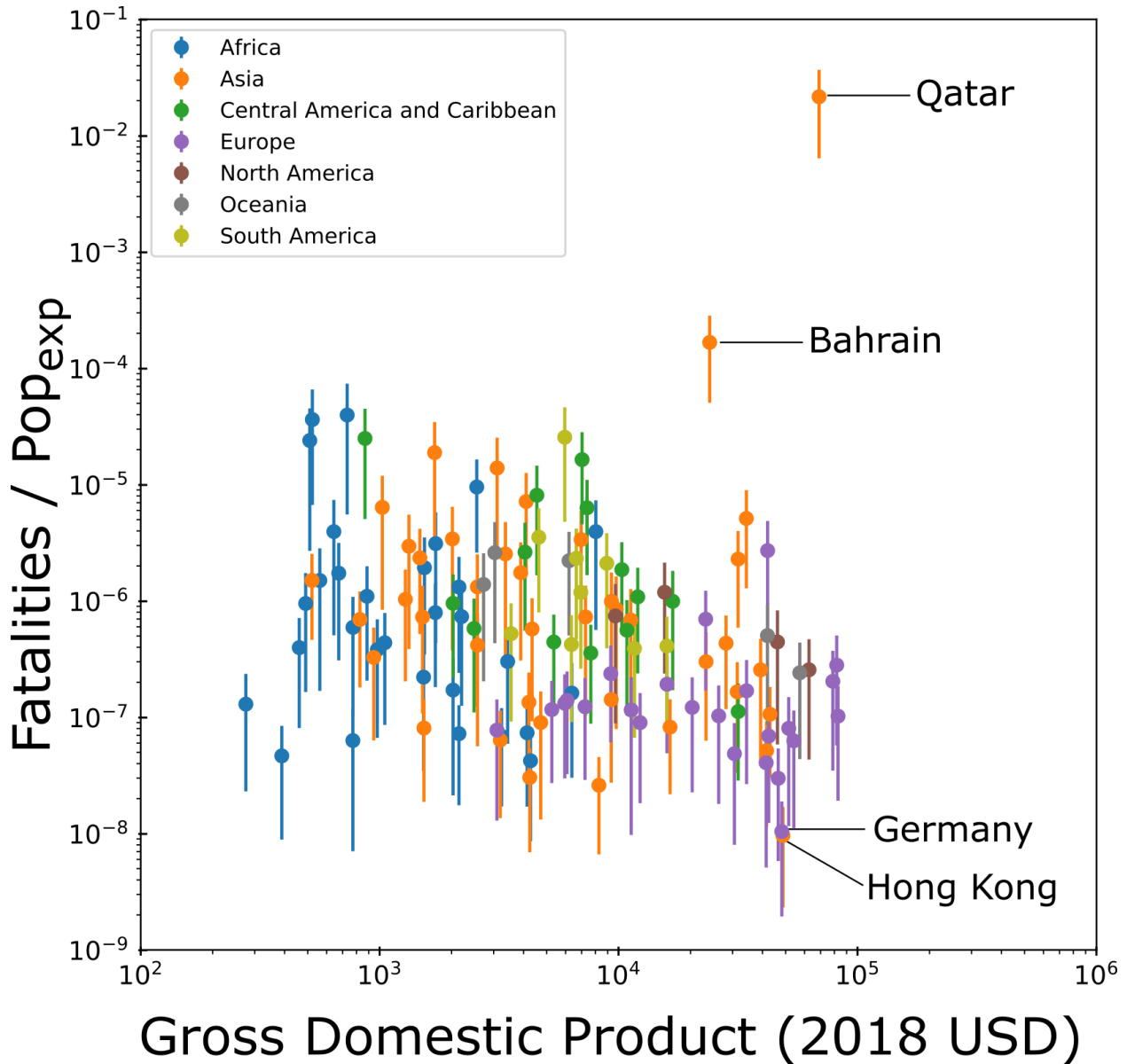
*Figure 8: Gross Domestic Product per capita (World Bank, 2018) compared with the number of landslide fatalities per unit exposure.*

While these results provide an independent estimate of landslide hazard and exposure across
480    the globe that does not rely on a specific inventory, there are still assumptions and limitations
that should be considered to put these results in appropriate context.

The most important caveat associated with this data is that Nowcasts do not represent a
guarantee of a landslide. The LHASA model Nowcasts (Kirschbaum and Stanley 2018) are
issued when there is an increased likelihood of a rainfall-triggered landslide, meaning the
485    estimates of exposure represent the relative likelihood of exposure to landslides, rather than the
reported impacts. As such, Nowcast number is a proxy for landslide hazard, rather than a
quantifiable landslide hazard. However, we suggest that this disadvantage is more than offset

by the global homogeneity and comparability of the Nowcast output. In addition, since the nowcast-based estimates of hazard are based on historical rainfall data, they do not provide

490 effective prediction of future exposure to hazard. This is particularly important given the potential for climate change to affect rainfall-driven hazards (Kleinen & Petschel-Held 2007). Our model estimates of exposure would also fail to capture rainfall driven exposure to landslide hazards in periods outside of the IMERG v06B record (pre 2001), including major rainfall-driven landslide events resulting from the 1998 El Nino event (Coe et al. 2004, Ngecu & Mathu 1999). We stress

495 that the model outputs are representative of the historical period under analysis, rather than strictly speaking a long-term average.

Additionally, since we do not have global data to quantify the vulnerability of settlements and infrastructure to landslide hazard, we cannot quantify the risk and impacts associated with landslide hazard. For example, data on fatalities associated with landsliding (Froude & Petley,

500 2018; Petley, 2012) quantifies the impacts, and while we can express our outputs in terms of relative proportion of population exposed to hazard, the lack of vulnerability data in our study represents an unconstrained source of variability if we compare those two datasets. Moreover, since the Nowcast output does not capture information about the size of a potential landslide in a given area, there may be differences in the severity of the landslide events that occur

505 depending on local factors (e.g. topography).

We note that we do not identify specific hospitals or schools as exposed to landslides. The resolution of our analysis remains coarse for individual points, and identifying specific locations could lead to overconfidence in exposure estimates. We acknowledge the importance of downscaling exposure estimates to those points, and suggest it is another important future

510 direction for landslide exposure estimation.

The resolution of the Nowcast data also presents challenges to the interpretation. While a Nowcast estimate for a 30 arc-second x 30 arc-second grid cell provides an estimate of the landslide hazard therein, it does not provide information about where exactly a landslide may occur. Since infrastructure and population are unlikely to be evenly distributed within a grid cell

515 (and are likely to be located further from areas of highest landslide susceptibility if risk mitigation measures have been adopted), elements that we describe as 'exposed to landslide hazard' may never actually be so. Given the resolution of our input hazard data, we suggest that it is challenging to provide a more finely resolved estimate. This does highlight the need for effective downscaling methods that can be applied to coarse resolution rainfall data to assess local

520 landslide hazard. We hope to address this in future work. In addition, the LHASA model only models rapid landslide failures in natural settings. This means it does not capture landslides resulting from anthropogenic influence or slow-moving landslide events, which lead to a significant number of fatalities every year (Petley, 2012). Constraining exposure to this kind of failure is another important subject for future studies.

525 The value of a homogenous global dataset is highlighted when comparing the relative exposure of population to landslide hazard based on our estimates with the GDP cost associated with landslides derived from Dilley et al. (2005). The prior study is based upon the EM-DAT inventory of damaging landslides, but the complete absence of data for countries in sub-Saharan Africa

530 (see Supplementary Table 1) contrasts strongly with our results, which suggest that there is a significant proportion of the population in many sub-Saharan African countries exposed to landslide hazard.

## 5. Conclusions

Through combining rainfall, topography and other satellite-derived data, we have developed a long-term estimate of landslide hazard across the globe, which we have utilised to estimate the
535 exposure of population and infrastructure to rainfall induced landslides. These estimates are globally consistent, and compare favourably with existing global datasets. When used in conjunction with datasets of landslide fatalities we can provide a nuanced picture of where and when landslides are most impactful. Our data highlights the importance of landslides in small, mountainous nations and islands; while the absolute numbers of fatalities may be smaller, these
540 represent locations with extremely high hazard and exposure. Further work is necessary to both test these results in a range of settings as well as to explore how global estimates can be downscaled and compared to more local estimates.

## Acknowledgements

All material necessary to replicate these results can be found in the supplementary material.
545 The authors have no conflicts of interest, financial or otherwise. D.K. and T.S. are supported by a NASA DISASTERS program grant 18-DISASTER18-0022. R.E. is supported by a NASA Postdoctoral Fellowship administered by Goddard Space Flight Center. All authors were involved in study conceptualisation and writing of the manuscript. R.E. and T.S. carried out modelling and analysis. Map data copyrighted OpenStreetMap contributors and available from
550 https://www.openstreetmap.org.

## References

Barrington-Leigh, C., & Millard-Ball, A. (2017). The world' s user-generated road map is more than 80 % complete. *PLOS One*, *12*(8), 1–20. https://doi.org/10.1371/journal.pone.0180698
Carrao, H., Naumann, G., & Barbosa, P. (2016). Mapping global patterns of drought risk : An
555 empirical framework based on sub-national estimates of hazard , exposure and vulnerability. *Global Environmental Change*, *39*, 108–124. https://doi.org/10.1016/j.gloenvcha.2016.04.012
Coe, B. J. A., Godt, J. W., & Tachker, P. (2004). Map showing recent (1997-98 El Niño) and historical landslides , Crow Creek and vicinity , Alameda and Contra Costa Counties ,
560 California. Denver, CO.
De Bono, A., & Chatenoux, B. (2014). *A Global Exposure Model for GAR 2015, UNEP/Grid, Geneva. Background Paper prepared for the 2015 Global Assessment Report on Disaster Risk Reduction*. Geneva.
Dilley, M., Chen, R. S., Deichmann, U., Lerner-Lam, A. L., Arnold, M., Agwe, J., … Gregory, Y.
565 (2005). *Natural Disaster Hotspots A Global Risk Analysis*. *Disaster Risk Management Series*. https://doi.org/10.1080/01944360902967228
Doxsey-Whitfield, E., MacManus, K., Adamo, S. B., Pistolesi, L., Squires, J., Borkovska, O., & Baptista, S. R. (2015). Taking Advantage of the Improved Availability of Census Data: A First Look at the Gridded Population of the World, Version 4. *Papers in Applied Geography*,
570 *1*(3), 226–234. https://doi.org/10.1080/23754931.2015.1014272

Froude, M. J., & Petley, D. N. (2018). Global fatal landslide occurrence from 2004 to 2016. *Natural Hazards and Earth System Science*, *18*, 2161–2181.

Guha-Sapir, D., & CRED. (2019). EM-DAT: The Emergency Events Database.

Haklay, M. (2010). How good is volunteered geographical information? A comparative study of OpenStreetMap and Ordnance Survey datasets, *37*(1). https://doi.org/10.1068/b35097

Kirschbaum, D. B., Adler, R., Hong, Y., Hill, S., & Lerner-Lam, A. (2010). A global landslide catalog for hazard applications: method, results, and limitations. *Natural Hazards*, *52*, 561–575. https://doi.org/10.1007/s11069-009-9401-4

Kirschbaum, D., & Stanley, T. (2018). Satellite-Based Assessment of Rainfall-Triggered Landslide Hazard for Situational Awareness. *Earth's Future*, *6*(3), 505–523. https://doi.org/10.1002/2017EF000715

Kleinen, T., & Petschel-Held, G. (2007). Integrated assessment of changes in flooding probabilities due to climate change. *Climatic Change*, *81*, 283–312. https://doi.org/10.1007/s10584-006-9159-6

Meijer, J. R., Huijbregts, M. A. J., Schotten, K. C. G. J., & Schipper, A. M. (2018). Global patterns of current and future road infrastructure. *Environmental Research Letters*, *13*, 064006.

Monsieurs, E., Jacobs, L., Michellier, C., Basimike Tchangaboba, J., Ganza, G. B., Kervyn, F., … Dewitte, O. (2018). Landslide inventory for hazard assessment in a data-poor context: a regional-scale approach in a tropical African environment. *Landslides*, (May), 1–15. https://doi.org/10.1007/s10346-018-1008-y

Mooney, P., Corcoran, P., & Winstanley, A. C. (2010). Towards Quality Metrics for OpenStreetMap. *Proceedings of the 18th SIGSPATIAL International Conference on Advances in Geographic Information Systems*, 514–517.

Ngecu, W. M., & Mathu, E. M. (1999). The El-Nino-triggered landslides and their socioeconomic impact on Kenya. Environmental Geology, 38 (October), 277–284.

OpenStreetMap contributors. (2015) Planet dump [Data file from 24/06/2019]. Retrieved from https://planet.openstreetmap.org.

Petley, D. (2012). Global patterns of loss of life from landslides. *Geology*, *40*(10), 927–930. https://doi.org/10.1130/G33217.1

Petley, D. N., Hearn, G. J., Hart, A., Rosser, N. J., Dunning, S. A., Oven, K., & Mitchell, W. A. (2007). Trends in landslide occurrence in Nepal. *Natural Hazards*, *43*, 23–44. https://doi.org/10.1007/s11069-006-9100-3

World Bank. "Population" World Development Indicators, The World Bank Group, 2018, data.worldbank.org/indicator/SP.POP.TOTL

World Bank. " GDP (current US$)" World Development Indicators, The World Bank Group, 2018, data.worldbank.org/indicator/NY.GDP.MKTP.CD